1.5.5.9 Band structure

1.5.5.9.1 Introduction

If X is a non-magnetic element then compounds of the form X_2MnZ have localised moments close to 4 μ_B on the Mn atoms. Experiment shows that the interactions giving rise to long-range magnetic order are indirect (RKKY) and can extend up to at least 7 nearest Mn neighbours [88W1]. Models put forward to interpret magnetic properties have attributed specific roles for the X and Z atoms. Usually the X atoms are considered to determine the lattice parameter and the Z atoms the conduction electron concentration. However, experiments, particularly on quaternary systems, have demonstrated that both the X and Z atoms play a similar role in establishing the magnetic properties. Furthermore, the magnetic properties are primarily determined by the conduction electron concentration. A further experimental observation indicates that the d electrons do not participate in the Fermi surface. Band structure calculations have been put forward to account for the bulk properties, but as yet there has been little comparison with microscopic investigations.

X_2YZ X = 3d, 4d; Y = 3d

X = 8A: Co, Ni; Pd; 1B: Cu
Y = 7A: Mn; 1B: Cu
Z = 3B: Al; In; 4B: Sn; 5B: Sb

Table 105. Calculated and experimental lattice constants of ferromagnetic (AFII in the case of Pd_2MnIn) Heusler alloys, calculated heats of formation ΔH, calculated magnetic moments of Mn in Heusler alloys p_{Mn} and calculated experimental saturation moments, p_s^{calc} and p_s^{exp}. Total sublattice moment of Pd_2MnIn is 4.04 μ_B [83K4].

X_2MnY	a_{calc} [Å]	a_{exp} [Å]	ΔH [eV]	p_{Mn} [μ_B]	p_s^{calc} [μ_B]	p_s^{exp} [μ_B]
F-Co_2MnAl	5.68	5.76	– 1.55	2.74	4.05	4.01 ± 0.05
F-Cu_2MnAl	5.85	5.95	– 0.35	3.36	3.38	3.6 – 4.1
F-Co_2MnSn	5.95	6.00	– 0.79	3.13	5.02	5.08 ± 0.05
F-Ni_2MnSn	5.99	6.05	– 0.93	3.39	3.75	4.05
F-Cu_2MnSn	6.13	6.17	0.3	3.52	3.61	4.11
AFII-Pd_2MnIn	6.37	6.37	– 0.98	3.90	0	0
F-Pd_2MnSn	6.35	5.38	– 1.60	3.78	3.86	4.23 ± 0.1
F-Pd_2MnSb	6.34	6.42	– 1.54	3.83	4.0	4.4 ± 0.1

Table 106. Magnetic moments of Mn atoms for ferromagnetic, p_{ferro}, AFI, p_{AFI} and AFII, p_{AFII}, moment alignments. Total-energy differences ΔE_1 between ferromagnetic and AFI moment alignments, and ΔE_{II} between ferromagnetic and AFII moment alignments, are also shown [83K4].

X_2MnY	p_{ferro} [μ_B]	$p_{AF\,I}$ [μ_B]	$p_{AF\,II}$ [μ_B]	ΔE_I [meV]	ΔE_{II} [meV]
Co_2MnAl	2.74	3.0	2.97	– 195.9	– 157.8
Cu_2MnAl	3.36	3.26	3.19	– 123.1	– 183.7
Co_2MnSn	3.13	3.26	3.21	– 268.7	– 244.9

X_2MnY	p_{ferro} [μ_B]	$p_{AF\,I}$ [μ_B]	$p_{AF\,II}$ [μ_B]	ΔE_I [meV]	ΔE_{II} [meV]
Ni_2MnSn	3.39	3.35	3.35	– 81.6	– 57.1
Cu_2MnSn	3.52	3.36	3.39	– 38.1	– 59.9
Pd_2MnIn	3.87	3.89	3.90	– 13.6	6.8
Pd_2MnSn	3.78	3.80	3.79	– 82.5	– 55.1
Pd_2MnSb	3.83	3.82	3.78	– 1.4	– 20.4

Table 107. Occupation numbers q_1 of s, p and d bands in Heusler alloys for majority (↑) and minority (↓) spin electrons. Numbers are for calculated ground states - all ferromagnetic except for Pd_2MnIn, which is AFII. The latter occupation numbers are for one sublattice only. f-state contributions are 0.3 - 0.4 (not listed). Last two columns are Fermi-level state densities in eV^{-1} [83K4].

X_2MnY	$(q_s)\uparrow$	$(a_p)\uparrow$	$(q_d)\uparrow$	$(q_s)\downarrow$	$(q_p)\downarrow$	$(q_d)\downarrow$	$[N(E_F)]\uparrow$	$[N(E_F)]\downarrow$
Co_2MnAl	1.35	1.76	12.78	1.37	1.92	8.57	1.4	0.2
Cu_2MnAl	1.48	1.93	14.16	1.50	1.99	10.73	0.5	0.7
Co_2MnSn	1.42	2.09	13.32	1.40	2.18	8.25	1.0	0.1
Ni_2MnSn	1.45	2.10	13.65	1.44	2.17	9.86	0.9	2.0
Cu_2MnSn	1.55	2.24	14.36	1.54	2.25	10.77	0.5	1.2
Pd_2MnIn	1.39	1.79	13.64	1.37	1.76	9.67	0.8	1.3
Pd_2MnSn	1.44	2.00	13.79	1.43	2.11	9.86	0.6	1.2
Pd_2MnSb	1.51	2.37	13.90	1.47	2.41	9.93	0.8	1.0

Table 108. Energy differences ΔE from Table 106, ΔE_I^{calc} and ΔE_{II}^{calc}, and "experimental" values from experimental exchange constants [83K4].

	ΔE_I^{calc} [meV]	ΔE_I^{exp} [meV]	ΔE_{II}^{calc} [meV]	ΔE_{II}^{exp} [meV]
Ni_2MnSn	– 82	– 72	– 57	– 80
Cu_2MnAl	– 123	– 173	– 184	– 172
Pd_2MnSn	– 83	– 66	– 55	– 55

Table 110. Equilibrium lattice constants a and magnetic moment p for the Ni-based Heusler alloys [88D1].

	a_{exp} [a.u.]	a_{theor} [a.u.]	$p_{Mn,\,theor}$ [μ_B]	$p_{tot,\,theor}$ [μ_B]	p_{exp} [μ_B]
Ni_2MnIn	6.072	6.049	3.43	3.91	4.40
Ni_2MnSn	6.057	6.023	3.43	3.73	4.05
Ni_2MnSb	6.000	6.001	3.13	3.39	3.27

Table 109. Calculated exchange constants J_1 and J_2 and calculated paramagnetic Curie temperatures, Θ_{calc}. $(T_C)_{exp}$ are measured in Curie temperatures and Θ_{exp} are measured paramagnetic Curie temperatures [83K4].

X_2MnY	J_1 [meV]	J_2 [meV]	Θ_{calc} [K]	$(T_C)_{exp}$ [K]	Θ_{exp} [K]
Co_2MnAl	0.840	0.062	808	697	
Cu_2MnAl	0.333	0.329	691	630	685
Co_2MnSn	0.874	0.188	1142	829	
Ni_2MnSn	0.221	– 0.015	296	344	337
Cu_2MnSn	0.097	0.107	220	530	
Pd_2MnIn	0.028	– 0.047	42	142	52
Pd_2MnSn	0.178	– 0.019	285	189	201
Pd_2MnSb	0.003	0.056	53	247	259

Table 111. The interband transitions resulting in the characteristic peaks seen in Figures 561, 564 and 567. The notations (↑) and (↓) represent the minority- and majority-spin bands, respectively [83K6].

		Ni_2MnSn	Cu_2MnAl	Pd_2MnSn
A	(↑)	12 → 13	14 → 15	13 → 14
	(↓)	13 → 14	17 → 18	17 → 18
B	(↑)	13, 14 → 15	14 → 15	13, 14 → 15
	(↓)			
C	(↑)	13, 14 → 19	14 → 19	14 → 19
	(↓)	18, 19 → 20	18, 19 → 20	
D	(↑)	4, 5, 6 → 20	5, 6 → 20	4, 5 → 20
	(↓)	4, 5, 6 → 20		4, 5 → 20

Table 112. Band parameters determined by Co_2MnSn [83I1]. The energy is measured in units of Rydberg. For notation see [81I1].

	Minority spin	Majority spin		Minority spin	Majority spin
dε(Mn)	– 0.388	– 0.677	V_4	0.0328	0.015
dγ(Mn)	– 0.423	– 0.697	V_5	0.018	0.05
dε(Co)	– 0.674	– 0.767	V_6	– 0.033	– 0.105
dγ(Co)	– 0.659	– 0.704	A(Mn)	– 0.05	0.345
$dd\sigma_1$	0.00124	0.02334	A(Co)	0.894	0.7
$dd\pi_1$	0.00021	0.00221	R_0(Mn)	3.3	3.3
$dd\delta_1$	0.0315	0.0045	R_0(Co)	3.2	3.4
$dd\sigma_2$	– 0.01798	– 0.0152	L_1(Mn)	0.91	0.96
$dd\pi_2$	0.01182	0.00913	L_1(Co)	0.96	0.96
$dd\delta_2$	0.00094	– 0.011	L_2(Mn)	1.56	1.56
$dd\sigma_{31}$	0.00288	– 0.00957	L_2(Co)	1.65	1.65

	Minority spin	Majority spin		Minority spin	Majority spin
$dd\pi_{31}$	– 0.00103	0.01	B(Mn)	– 0.58	– 0.63
$dd\delta_{31}$	0.00525	0.0069	B(Co)	– 0.542	– 0.54
$dd\sigma_{32}$	0.00088	0.00283	R_1(Mn)	3.78	3.78
$dd\pi_{32}$	– 0.00203	– 0.00499	R_1(Co)	3.68	3.4
$dd\delta_{32}$	0.00225	– 0.00051	L_3(Mn)	0.915	1.115
V_0	– 1.28	– 1.292	L_3(Co)	0.985	0.935
V_1	– 0.093	– 0.093	L_4(Mn)	1.38	1.38
V_2	– 0.015	– 0.009	L_4(Co)	1.38	1.58
V_3	0.037	0.065			

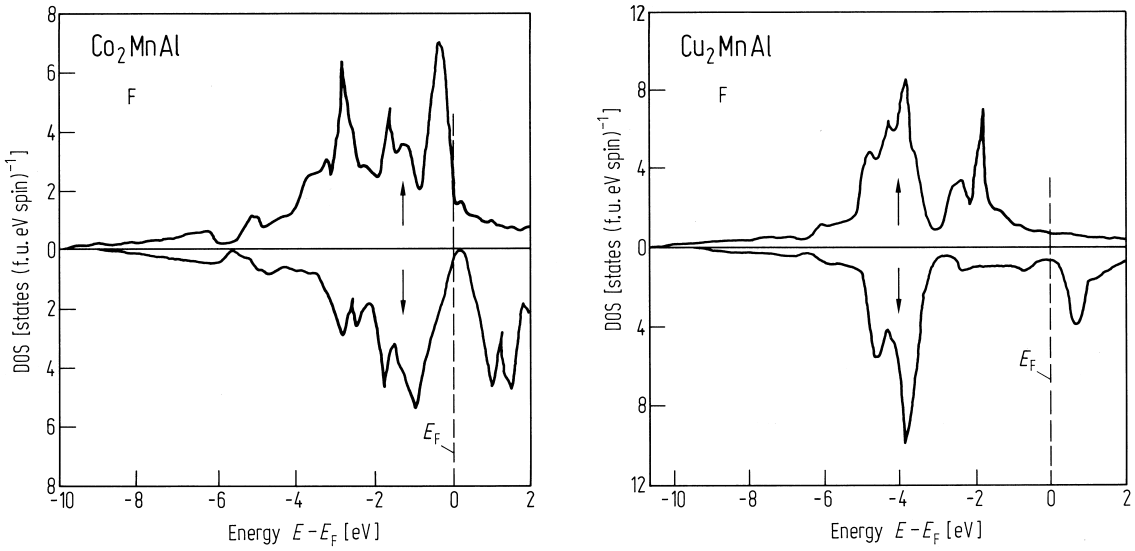

Fig. 499. Total majority (↑) and minority (↓) state densities per formula unit for ferromagnetic Co_2MnAl and Cu_2MnAl [83K4].

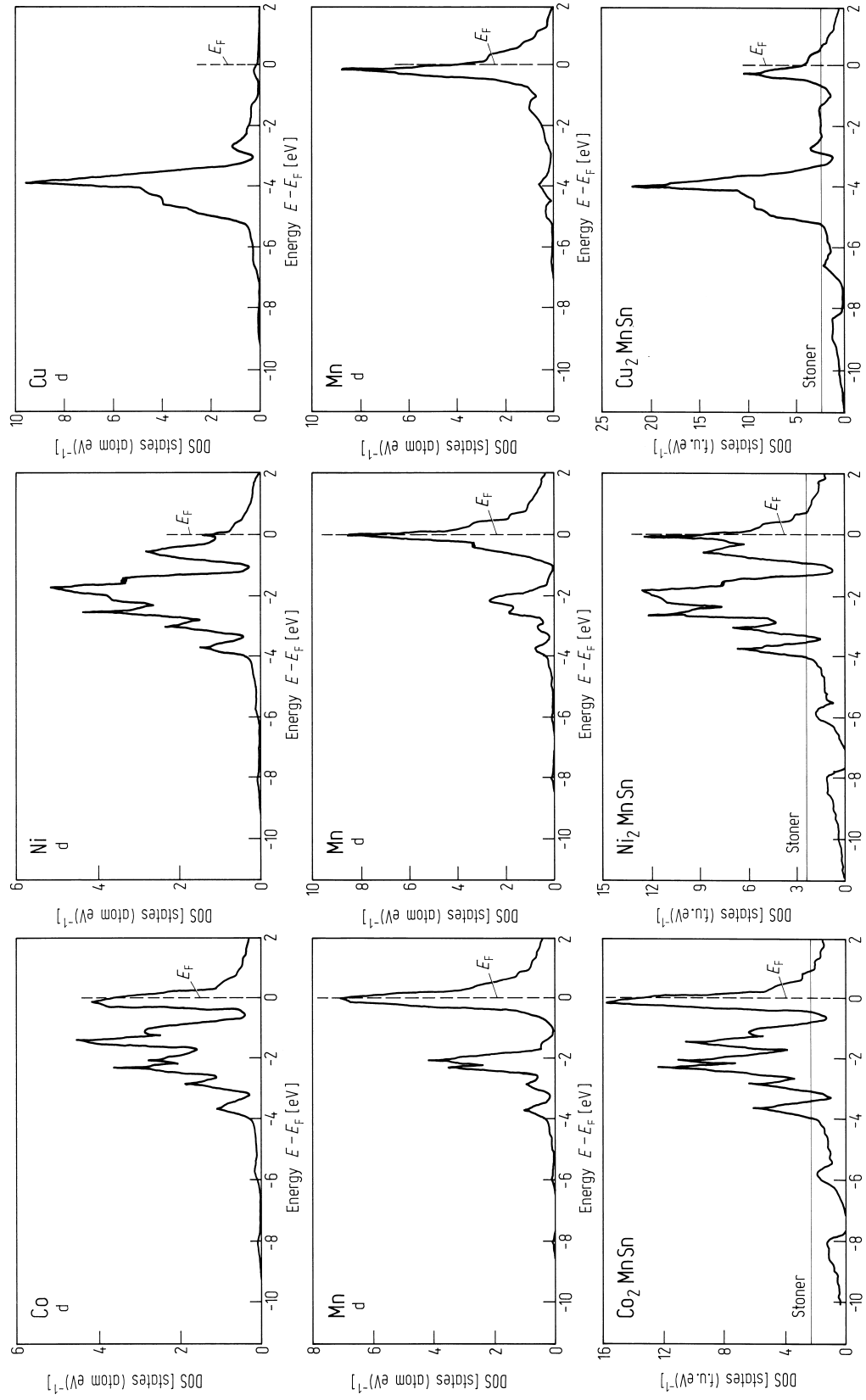

Fig. 498. Total state densities per formula unit of assumed nonmagnetic Co_2MnSn, Ni_2MnSn and Cu_2MnSn shown in lower panels. Site- and angular-momentum-projected d-state densities of the constituents shown in upper panels [83K4].

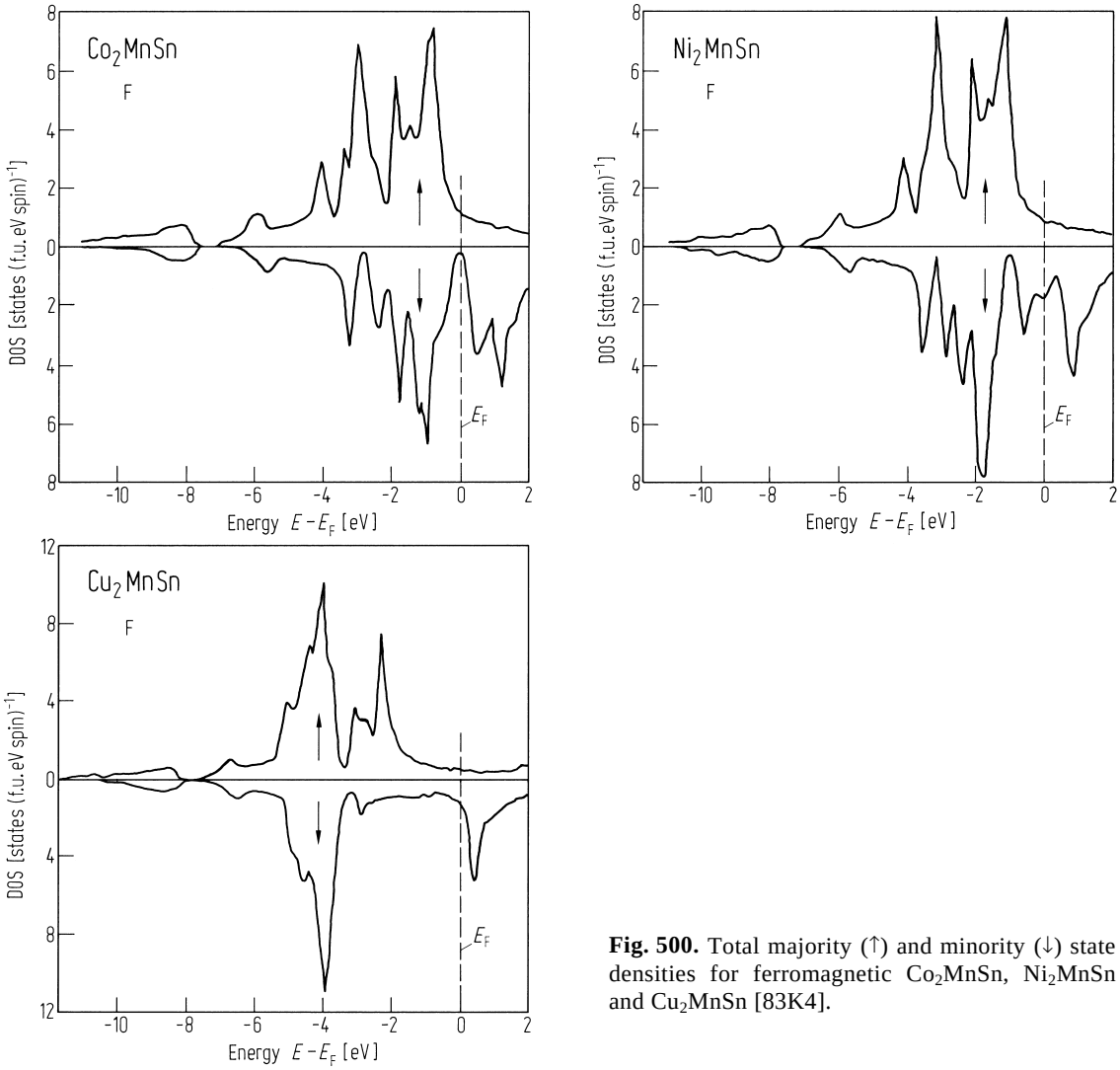

Fig. 500. Total majority (↑) and minority (↓) state densities for ferromagnetic Co_2MnSn, Ni_2MnSn and Cu_2MnSn [83K4].

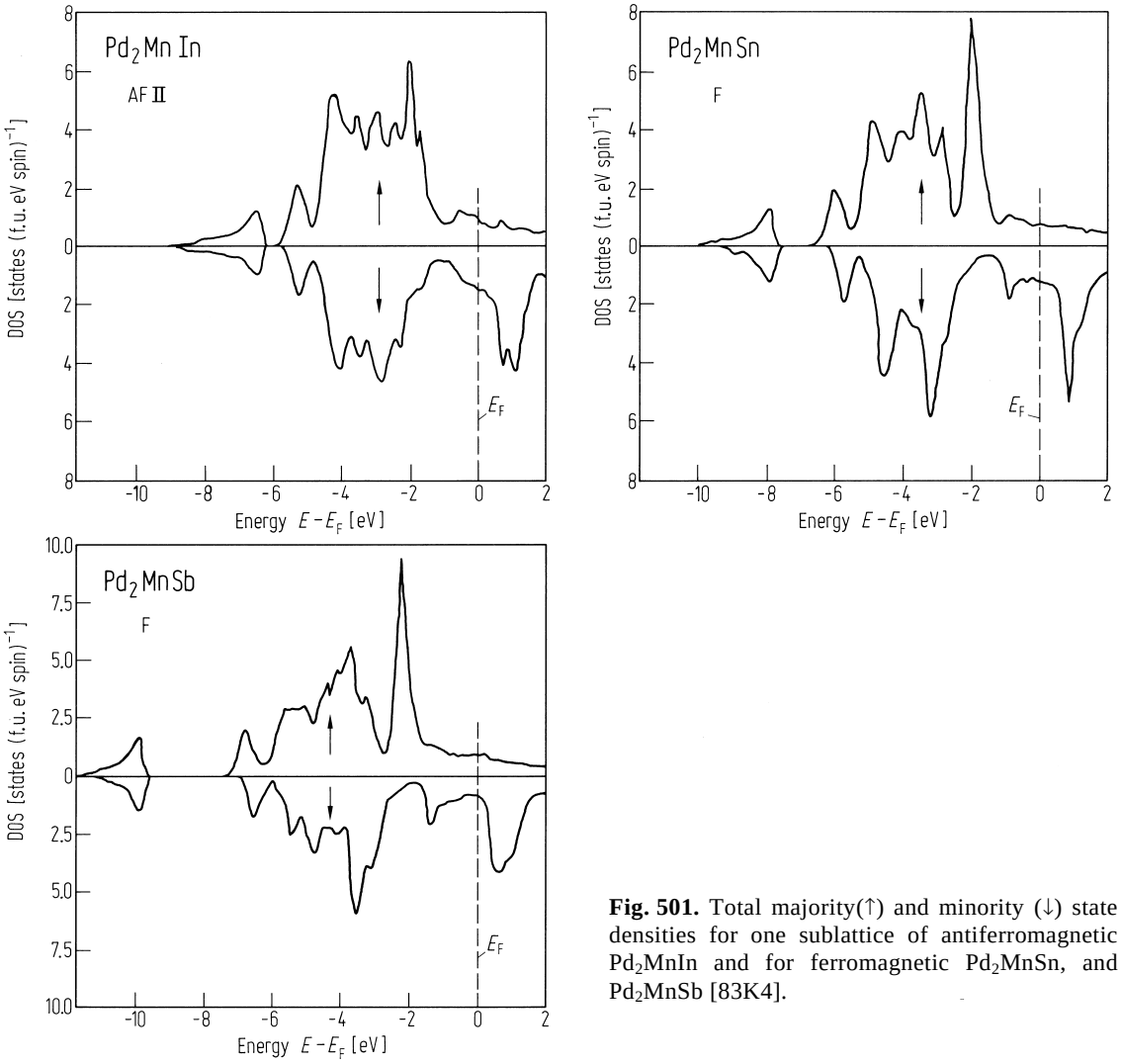

Fig. 501. Total majority(↑) and minority (↓) state densities for one sublattice of antiferromagnetic Pd_2MnIn and for ferromagnetic Pd_2MnSn, and Pd_2MnSb [83K4].

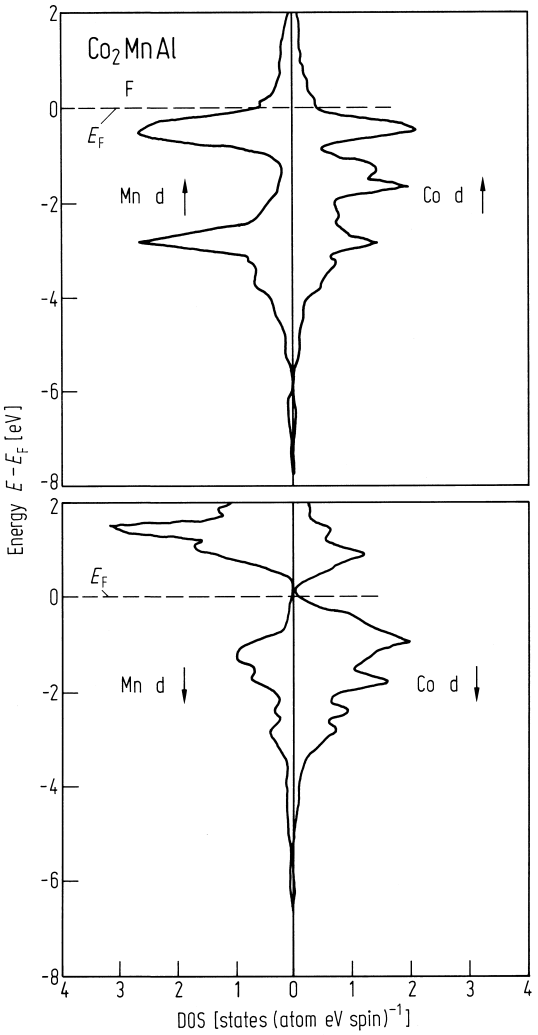

Fig. 502. Site- and spin-projected d-electron state densities for ferromagnetic Co_2MnAl [83K4].

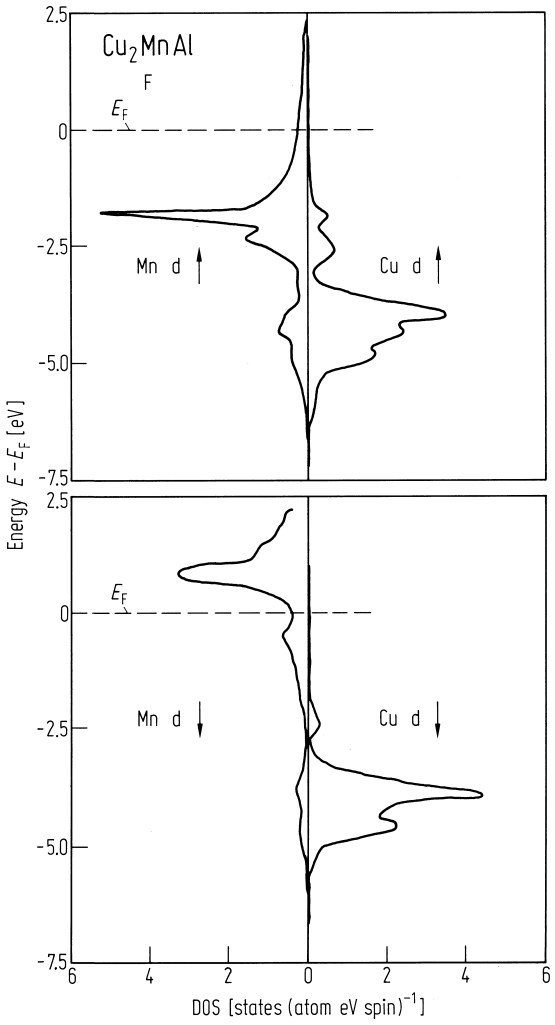

Fig. 503. Site- and spin-projected d-electron state densities for ferromagnetic Cu_2MnAl [83K4].

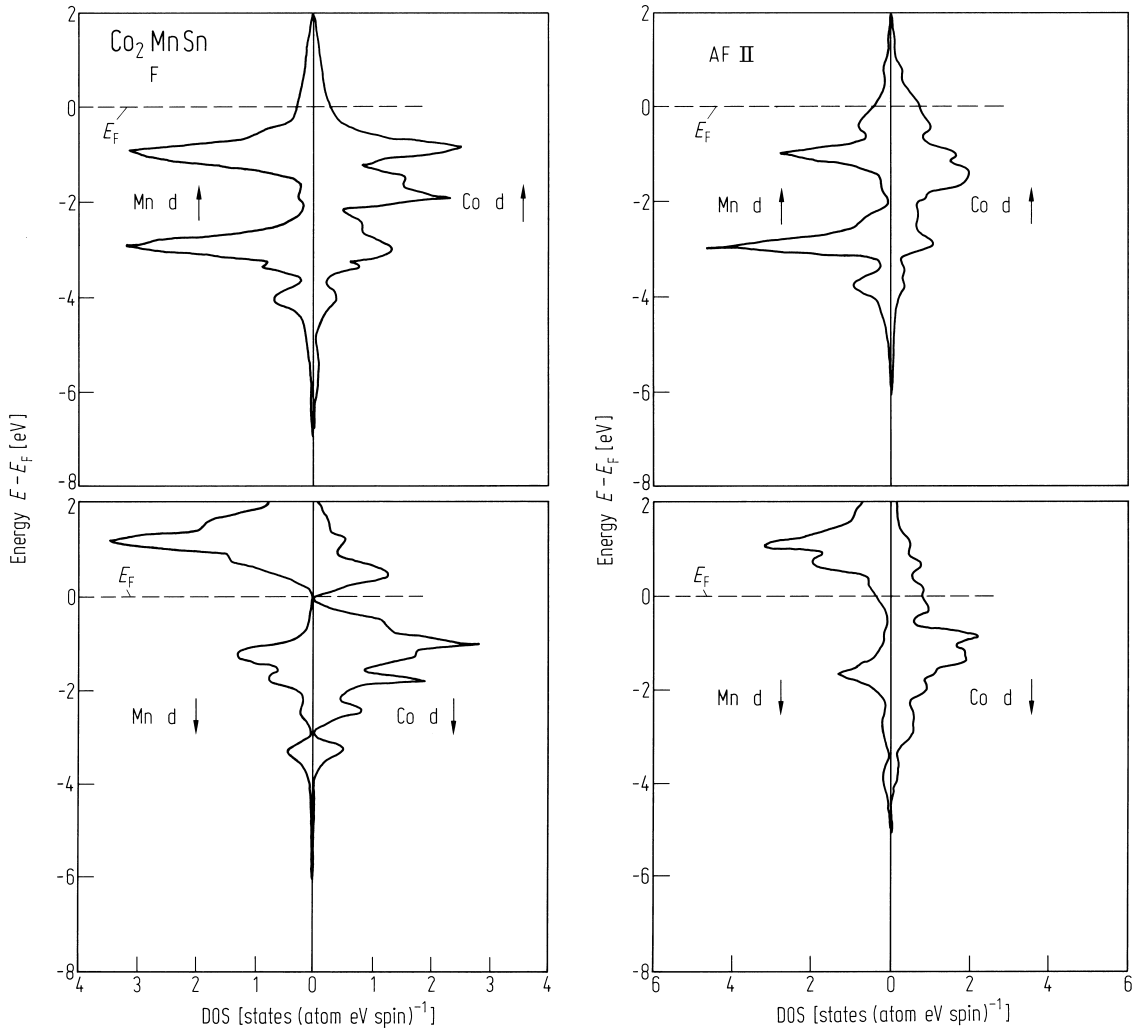

Fig. 504. Site- and spin-projected d-electron state densities for and ferromagnetic Co_2MnSn, and and antiferromagnetic Co_2MnSn [83K4].

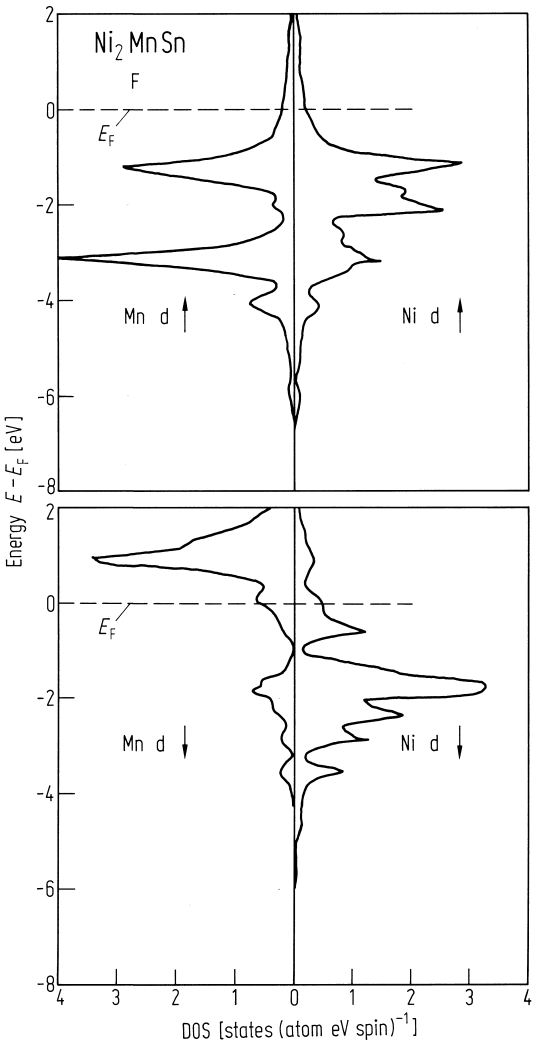

Fig. 505. Site- and spin-projected d-electron state densities for ferromagnetic Ni_2MnSn [83K4].

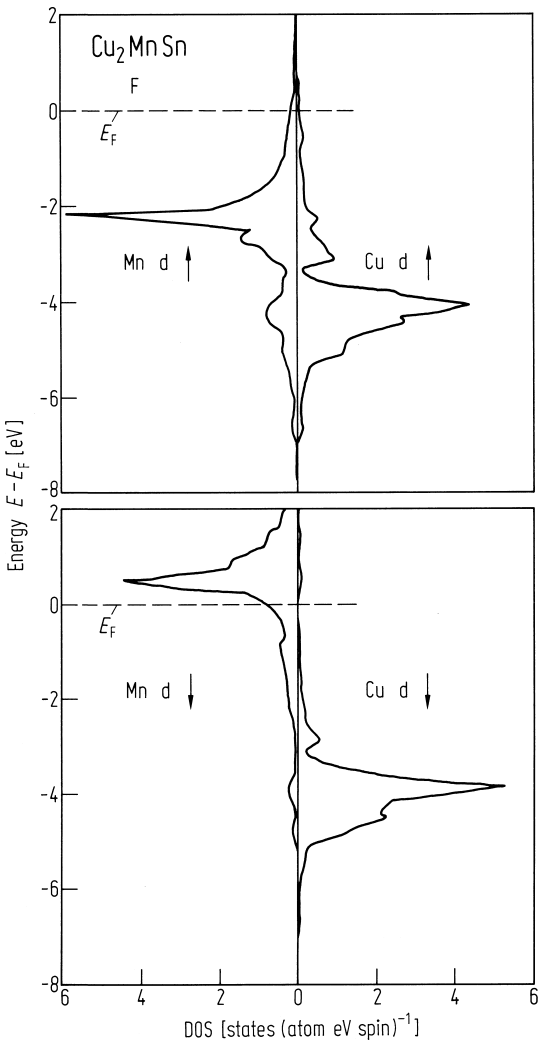

Fig. 506. Site- and spin-projected d-electron state densities for ferromagnetic Cu_2MnSn [83K4].

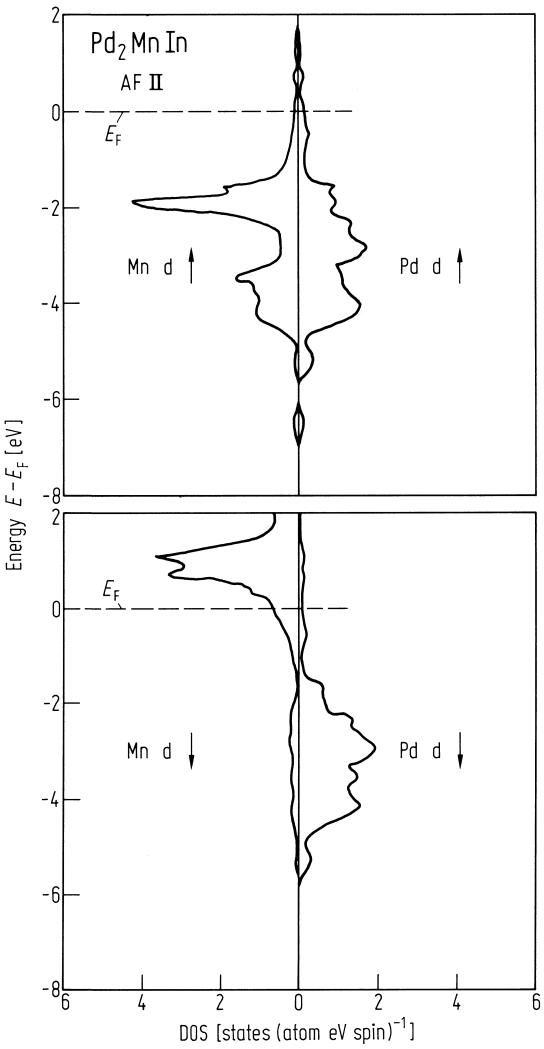

Fig. 507. Site- and spin-projected d-electron sublattice state densities for antiferromagnetic (AFII) Pd_2MnIn [83K4].

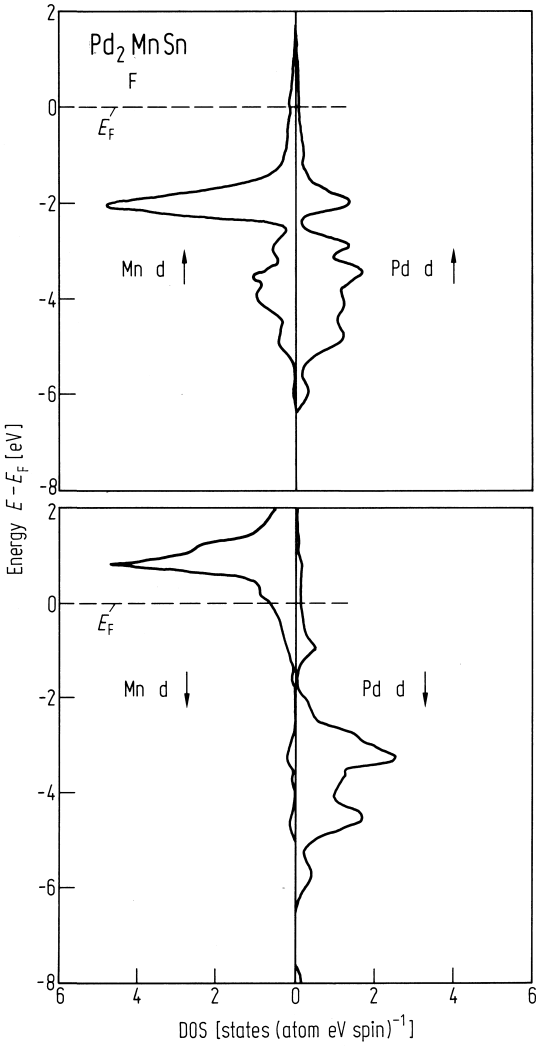

Fig. 508. Site- and spin-projected d-electron state densities for ferromagnetic Pd_2MnSn [83K4].

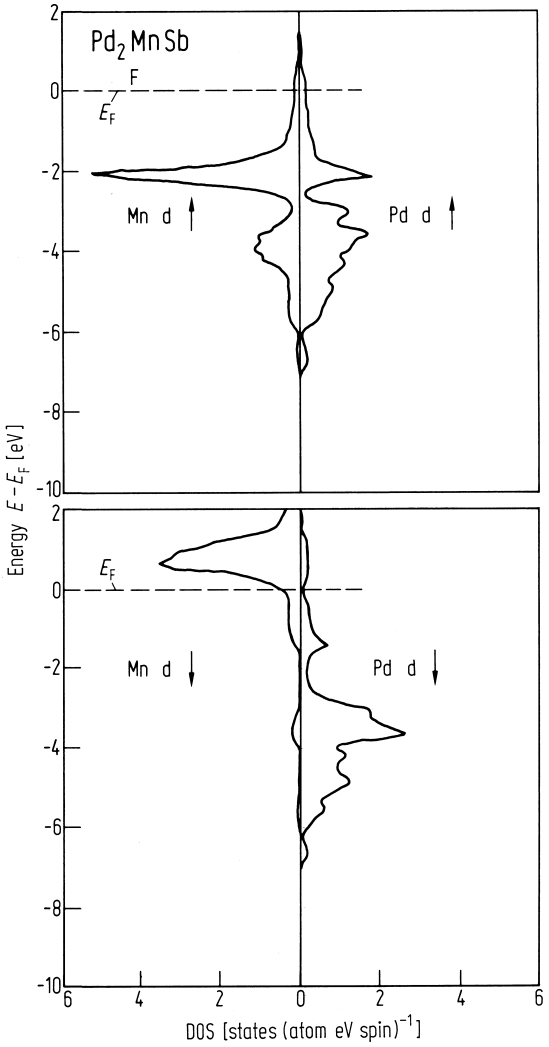

Fig. 509. Site- and spin-projected d-electron state densities for ferromagnetic Pd_2MnSb [83K4].

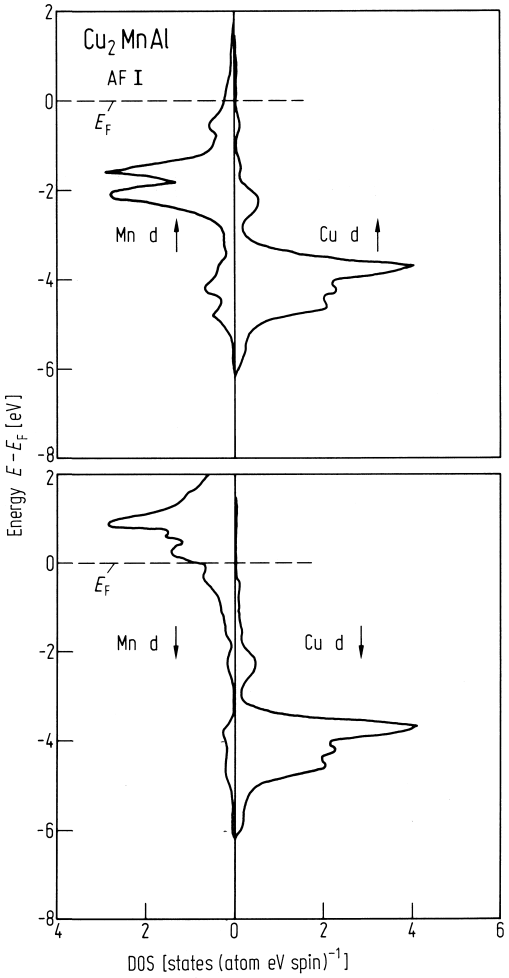

Fig. 511. Site- and spin-projected d-electron sublattice state densities for assumed antiferromagnetic (AFI) Cu_2MnAl [83K4].

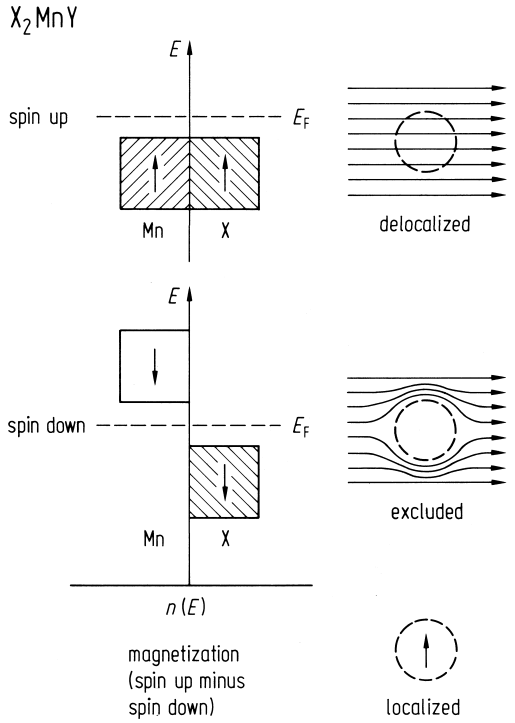

Fig. 510. Localised magnetic moment from delocalised electrons. Schematic diagram of up-spin and down-spin d-electrons in Heusler alloys (X_2MnY). Corresponding non-schematic state densities are shown in Figs. 502-509 [83K4].

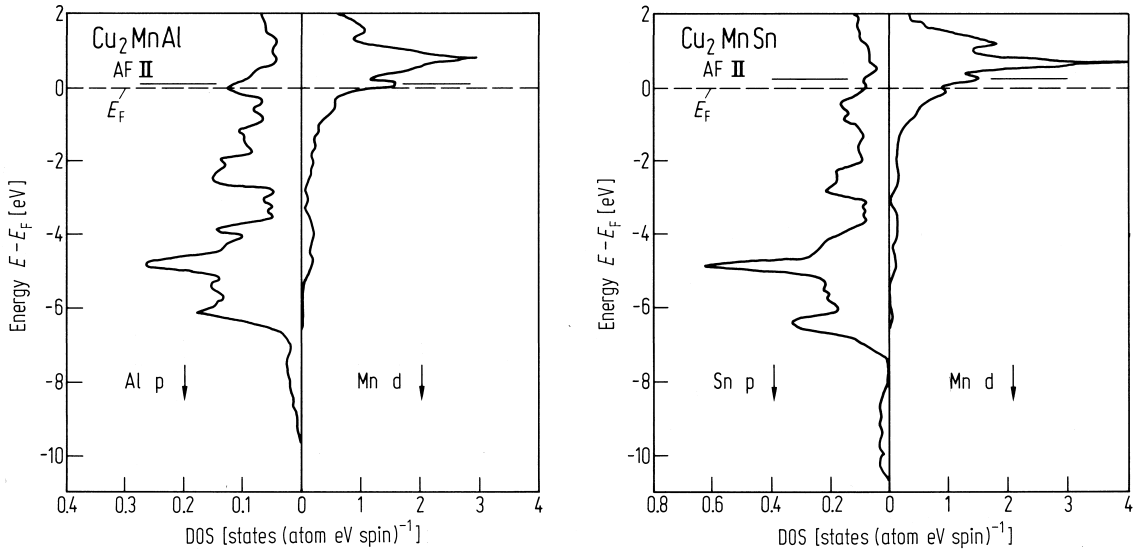

Fig. 512. Minority site- and spin-projected state densities of p and d electrons of Al and Mn respectively, in antiferromagnetic Cu_2MnAl and for Sn and Mn respectively, in antiferromagnetic Cu_2MnSn [83K4].